Microwave vs. Millimeter-Wave Propagation Channels: Key Differences and Impact on 5G Cellular Systems

Mansoor Shafi, Jianhua Zhang, Harsh Tataria, Andreas F. Molisch, Shu Sun, Theodore S. Rappaport, Fredrik Tufvesson, Shangbin Wu, and Koshiro Kitao

While we have a reasonable understanding of the propagation characteristics at microwave (< 6 GHz) frequencies, the same cannot be said for mmWave. The authors explain key differences in the propagation characteristics between the microwave and mmWave bands, and further give examples of how these differences impact 5G system design.

Abstract

Fifth generation cellular systems will be deployed in the microwave and millimeter–wave (mmWave) frequency bands (i.e., between 0.5–100 GHz). Propagation characteristics at these bands have a fundamental impact on each aspect of the cellular architecture, ranging from equipment design to real-time performance in the field. While we have a reasonable understanding of the propagation characteristics at microwave (< 6 GHz) frequencies, the same cannot be said for mmWave. This article explains key differences in the propagation characteristics between the microwave and mmWave bands, and further gives examples of how these differences impact 5G system design.

Introduction

In order to meet the high data rate requirements of fifth generation (5G) cellular systems (20 Gb/s), large bandwidths (up to 1 GHz) are needed that are not available in the sub-6 GHz (microwave) frequency bands. The millimeter-wave (mmWave) bands (30–300 GHz) are relatively unused, and have large available bandwidths attracting a lot of interest for 5G cellular access. However, the nature of radio propagation between microwave and mmWave frequencies is different, and this has a wide ranging impact on all system aspects — in particular, system performance, equipment design, signal processing requirements, and fundamental architectures of both the base station (BS) as well as the user equipment (UE). Almost all current cellular systems are deployed in the microwave bands. Therefore, a wealth of experience and measurement results are available; however, comparatively fewer measurements exist for the mmWave bands [1–5]. With the above discussion in mind, a natural question to ask would be: *What are the fundamental differences between the mmWave and microwave propagation channels, and what physical processes lead to such differences?* In this article, we present an overview of these key differences, and highlight their impact on 5G cellular system design.

Propagation channel models, which describe the statistics of small-scale and large-scale variations in different environments, are in turn determined by the characteristics of the different multipath components, that is, signal echoes that propagate from the transmitter to the receiver via different paths, *interacting* with the environment in various different ways. It is well known that the various propagation processes describing these interactions are frequency-dependent [1, 5–7]; this forms the physical basis of why we can anticipate different channel behaviors at different carrier frequencies. First and foremost, the free-space path loss increases quadratically with carrier frequency, f, when considering antennas with *frequency-independent gain* (e.g. shrinking the antenna aperture as frequency increases) at both link ends. In contrast to this, if the antennas at both link ends have a constant physical area and frequency-dependent gain, the path loss *decreases* with the square of f [6, 7]. Furthermore, specular reflections at a dielectric halfspace (representing ground reflections) are frequency-dependent only as far as the dielectric constant is frequency-dependent, while reflection at a dielectric *layer*, such as a building wall, depends on the electrical thickness of the wall, and thus on frequency. Having said this, it is not clear whether reflection coefficients increase or decrease with frequency. Conversely, transmission power *through* objects almost uniformly decreases with increasing frequency due to the presence of the skin effect in lossy media. Another two effects that have also drawn attention at mmWave frequencies are *diffraction* and *diffuse reflection*. The efficiency of diffraction strongly decreases with increasing frequency, as obstacles such as building walls or people introduce sharp "shadows." Conversely, diffuse scattering becomes more relevant as the surface roughness of common objects becomes comparable to the wavelength (more precisely, as the Rayleigh roughness becomes close to, or larger than, unity). In the extreme case, rough surfaces essentially diffuse radiation *uniformly* in all directions. A similar effect also occurs in *penetration through foliage*: as the leaves become comparable in size relative to the wavelength, signal penetration through the leaves decreases, while scattering off the leaves increases. Last but not least, the size of the first Fresnel zone (the area particularly vulnerable to shadowing objects) decreases with the

Mansoor Shafi is with Spark New Zealand; Jianhua Zhang is with Beijing University of Posts and Telecommunications; Harsh Tataria is with Queen's University Belfast; Andreas F. Molisch is with the University of Southern California; Shu Sun is with Intel Corporation; Theodore S. Rappaport is with New York University; Fredrik Tufvesson is with Lund University; Shangbin Wu is with the Samsung R&D Institute UK; Koshiro Kitao is with NTT DOCOMO, INC.

Digital Object Identifier:
10.1109/MCOM.2018.1800255

square root of the wavelength. For realistic simulations, all of these physical phenomena need to be incorporated into ray tracers and statistical models for research and system design. A major challenge for accurate ray tracing implementation will be to account for the physical features of buildings, as well as obtaining sufficiently high-resolution databases of the terrain, as standard databases only offer resolution on the order of a few meters, and thus do not show effects such as transitions from smooth windows to rough stucco, for example. Furthermore, the impact of these effects on overall (statistical) channel parameters greatly depends on the type of environment. For instance, in downtown urban centers with smooth glass/concrete building surfaces, one can expect smaller frequency dependence than in suburban environments, where houses have stucco surfaces and surrounding vegetation.

Large-Scale Propagation Behavior

Path Loss

Path loss governs the coverage distance and interference levels (a key factor in determining the signal-to-interference-plus-noise ratio, SINR) of a cellular system. Path loss models have varying degrees of complexity and accuracy, and may also include dependence on antenna heights, as well as operational scenarios (e.g. urban, rural). Due to their frequency dependence and the impact of antenna gains, path loss models are different for microwave and mmWave bands [1, 5–7]. The statistical deviation of the path loss model fit from measured field data is expressed by the root mean square error between actual and predicted signal strength (local average) over distance, and is interpreted as an estimate of the *shadow fading* standard deviation, σ (in dB).

The atmosphere, including oxygen, rain, and so on, induces additional frequency-dependent attenuation to signal power, primarily at mmWave. Losses caused by oxygen and light rain are negligible at microwave frequencies as well as for small cell distances at mmWave bands (except for frequencies around 60 GHz, where oxygen absorption creates about a 20 dB/km loss), but heavy rain/hail/fog may induce severe loss at mmWave frequencies. Unlike today's microwave systems, 5G cellular systems will utilize extremely directive, high gain antennas to overcome weather effects and free space loss due to frequency. Researchers have proposed various statistical path loss models for mmWave frequencies, such as the Stanford University Interim (SUI) model adopted for mmWave frequencies [1], but the two most popular models are the *ABG* and *CI* models. Expressions for both models are detailed in [1, 5]. The ABG model is inherited and extended from the legacy floating-intercept model, and has three parameters. Two of the parameters show dependence on the link distance and frequency, while the other is an optimized offset value based on the specific measured dataset used to create the model. The three parameters are obtained through a least squares fit of measured data to minimize σ. In contrast, the CI model uses a 1 m close-in free space reference and has only one parameter, the path loss exponent (PLE), offering much less computational complexity than the ABG model when determining model parameters, while providing comparable fitting accuracy with much better stability and accuracy when extrapolated outside the distance range for the measured data, as demonstrated in [5]. Besides the CI model, model extensions use frequency-dependent PLE (the CIF model) or a BS-height-dependent PLE (the CIH model).

The ABG and CI models are applicable to both microwave and mmWave bands [4, 11]. To provide an intuitive comparison of path loss models between microwave and mmWave frequencies, we plot the omnidirectional path loss at 2 GHz and 100 GHz using Third Generation Partnership Project/International Telecommunication Union (3GPP/ITU) (ABG) and NYUSIM (CI) channel models for the urban microcell (UMi) scenario, as illustrated in Fig. 1a. The PLEs in the NYUSIM model are obtained from field measurements in UMi environments [5]. Figure 1a shows that the free space loss in the first meter is approximately 34 dB greater at 100 GHz compared to 2 GHz, as captured by Friis' law. Moreover, by comparing the path loss models in the same environment but with different frequencies (excluding the curves with breakpoints), it is seen that the path loss lines at microwave and mmWave frequencies are almost parallel, meaning that there is *virtually no difference* in the path loss exponent *beyond the first meter of free space*, such that PLEs are of comparable values and independent of frequency [1, 5,7].

Probability of Line of Sight

This depends on the distance between the BS and UE, as well as the surrounding physical structures in the propagation environment (e.g., density and heights of buildings close to the BS and UE). It is important to note that the line of sight (LoS) probability *does not depend on carrier frequency*. In the 3GPP/ITU channel models, it is applicable over 0.5–100 GHz. The NYUSIM model proposes a *new* model that more accurately predicts the LoS probability, especially at large distances for UEs [5].

Shadow Fading

Shadowing is significantly more pronounced at higher frequencies due to the higher losses induced by diffraction. One needs to distinguish between *three* different types of shadow fading:

1. Environmental shadowing, which is experienced as the UE moves along a trajectory. In this case, power variations occur as the UE moves into and out of regions that are covered by the BS via efficient reflection processes.
2. Shadowing induced by environmental objects: Whenever a multipath component (MPC) is blocked by another person or an object (e.g., a car), the path becomes strongly attenuated.
3. Self-shadowing by the person holding the UE, which depends on rotation, and change of hold (e.g., to ear vs. in front of torso). Detailed measurement-based models have been developed over the past six years.

For all of these effects, we find that the shadow fading variance increases with frequency. Recent work [8] has also shown that for microcells, the path loss coefficient depends on the street orientation, leading to strong variations of received signal strength between streets at the *same distance*

The impact of these effects on overall (statistical) channel parameters greatly depends on the type of environment. For instance, in downtown urban centers with smooth glass/concrete building surfaces, one can expect smaller frequency dependence than in suburban environments, where houses have stucco surfaces and surrounding vegetation.

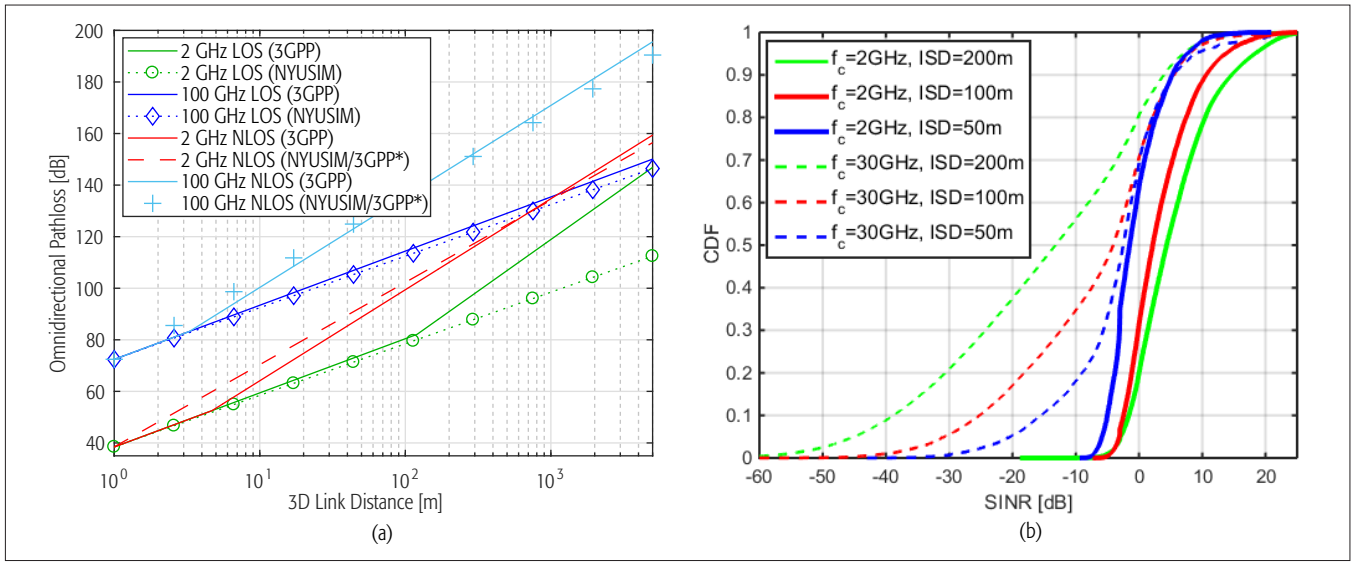

Figure 1. a) UMi omnidirectional path loss at 2 GHz and 100 GHz; b) SINR comparison between 2 and 30 GHz with different ISDs. One UE is assumed with a 64- and 256-element cross-polarized array at 2 and 30 GHz.

from the BS. If such variations are interpreted as environmental shadowing, shadowing variances also increase with distance. While this effect is present in the microwave frequencies, it is *more pronounced* for mmWaves.

Penetration Loss

For UEs in indoor environments, a channel model with penetration loss becomes vital. While penetration loss for sub-6 GHz frequencies is mostly constant [9, 10], it increases at mmWave frequencies. Moreover, very different types of penetration losses were observed for urban environments relative to suburban one [11]. References [4, 11], using a weighted average of the transmission through different materials available in urban and suburban environments, result in a dynamic range of penetration loss between 12 to 32 dB from 3 to 100 GHz for their low loss model, and between 30 to 60 dB for their high loss model.

Cell Ranges and Intercellular Interference

Network densification will be a key aspect of 5G cellular systems. By reducing the cell size, spectrum resources can be reused in different geographical areas, increasing the per-user throughput in a cell. As a result, the UMi scenario is vital to 5G New Radio (NR) channel modeling and system design. A typical cell range of UMi is defined as 200 m in both microwave and mmWave bands in 3GPP/ITU. Figure 1b presents the SINR comparison between 2 GHz and 30 GHz cellular networks. The simulation is performed in a wrapped 57-cell UMi network layout. At 2 GHz [10], each cell is equipped with a 64-element cross-polarized array with discrete Fourier transform precoding, while at 30 GHz [11], an array of 256 cross-polarized elements is employed. It can be observed that in the 2 GHz system, the SINR *drops* as inter-site distance (ISD) shrinks. On the contrary, SINR in the 30 GHz network *grows* when the ISD decreases from 200 m to 50 m. This finding implies that at 2 GHz, the noise power is negligible and the dominant performance limiting factor is intercellular interference (ICI). As such, the difference between the signal-to-interference ratio (SIR) and SINR is *small*. At 30 GHz, the higher propagation loss for omnidirectional antennas leads to a requirement for highly directive antennas [1, 5]. Consequently, ICI plays a less significant role relative to the noise power, *increasing* the gap between SIR and SINR. These different characteristics naturally impact the focus of system design in microwave and mmWave bands. Overall, the aim of microwave network coordination is how BSs cooperate to mitigate mutual interference, while coordination at mmWave must focus on effective link switching among coordinated BSs to retain coverage with UE mobility.

Bandwidth Dependency

Bandwidth has a large impact on how the BS and UE experience the mmWave channel. With a larger bandwidth, the *delay resolution increases*, and hence it is easier for the BS and UE to resolve the present MPCs. As a result, the *channel statistics also change with the bandwidth*. In [11], the bandwidth dependency of channel parameters was discussed for various environments. An important observation was that parameters such as delay spread (DS) and angular spread (AS) *change as the bandwidth changes*. More measurements are needed to confirm this trend over a wide range of scenarios. This implies the necessity to adjust the beamforming coefficients over the frequency band when using wider bandwidths. Also, the *K*-factor for each resolvable delay bin tends to increase with delay resolution, and there is a shift in the small-scale fading statistics due to the possibility of resolving the dominating component. The directional DS and AS are *shorter* than the corresponding omnidirectional values, and there are significant variations in the directional spreads between different frequencies at lower bandwidths. For large bandwidths, directional spreads seem to be in between spreads experienced at various frequencies having lower bandwidths [12].

Cluster Numbers and Hybrid Beamforming Performance

At mmWaves, an important characteristic is the relatively *small* number of *dominant* MPCs in comparison to microwave frequencies. While significant diffuse scattering is anticipated from theoretical considerations, recent measurement campaigns in both indoor and outdoor environments have demonstrated that a high percentage of the received energy can be explained by *discrete* MPCs [1, 2]. An intrinsic limitation of most mmWave campaigns is the *non-coherent*) nature of the measurements with directional antennas, such that the *angular resolution* is limited by its narrow beamwidth. As a result, multiple MPCs may fall into the antenna beamwidth, but appear as a single MPC. It is thus difficult to state the *precise* number of contributing MPCs in a given propagation environment, and it is *not clear* whether channels are sparse in the sense of having a *small* number of MPCs. Nevertheless, mmWave channels *are sparse* in the sense that majority of the resolvable delay/angular bins *do not* contain MPCs with sufficient electromagnetic energy [1, 12]. Due to the above-mentioned effects, the angular (double-directional) characteristics of mmWave channels are significantly *different* from sub-6 GHz channels, and the higher directionality of mmWave antennas relative to comparable size below 6 GHz changes the interaction between BS/UE and the channel [1].

Like sub-6 GHz, MPCs at mmWave also have the tendency to occur in *clusters* (i.e., groups of MPCs that have similar angular and delay characteristics). This effect arises as the MPCs are created by the interaction of the transmit waveform with physical objects, such as a group of high rise buildings, or from the waveform undergoing similar waveguiding process in a corridor or a street canyon. Clusters can be extracted from channel measurement data via analysis of the multidimensional power spectrum and clustering algorithms [2]. Different propagation models have *different* definitions for clusters, as well as recommendations on the *numbe*r of clusters for a given propagation environment. For instance, the 3GPP/ITU channel model (and its extensions) defines a cluster as a group of MPCs with the *same* delay, and a power angular spectrum centered around a mean angle that itself is chosen as a random deviation from the LoS angle. Rather surprisingly, [11] states that even at mmWave, the number of MPCs within each cluster is 20, with a *fixed* number of clusters dependent on the operational scenario. In sharp contrast to this, the COST 259/273/2100 models define a cluster as a group of MPCs that all have similar parameters — delay, angle of arrival (AoA), and angle of departure (AoD) — while having parameters that are significantly distinct from those of other clusters in at least one dimension. Furthermore, the COST models, as well as the NYUSIM model, define the *number* of clusters as a *random variable* whose distribution parameters depend on the propagation scenario and environment. COST 259/273/2100 also models the appearance and disappearance of clusters via the concept of *random visibility region*s in the coverage area, so if a UE is in such a region, the cluster contributes to the CIR. This ensures *spatial consistency* when the UE moves along a trajectory. The NYUSIM model defines the concept of *time clusters*, where a group of MPCs traveling close in time can arrive from different angles, as well as *spatial lobes* which denotes primary AoDs/AoAs, where energy arrives over a short time period. Typically, the *Poisson distribution* is used to model the random number of clusters with a given mean. This is in line with recent measurements [12] that found an *average* number of 3.52 and 4.58 clusters for indoor and outdoor UMi non-LoS (NLoS) scenarios, respectively. Figure 2a depicts the corresponding CDFs of the number of clusters in both scenarios, where the positive Poisson distributions are illustrated as best fits. In contrast to the 3GPP/ITU model, a significantly *smaller number of clusters* is observed on average, providing indications of *channel sparsity*. The above differences in cluster numbers (and cluster definitions) have important consequences on the design of the mmWave transceiver architectures, as well as on its performance.

Since a *physically* small antenna aperture becomes *electrically* large at mmWave bands, mmWave systems are inherently more capable of focusing beams and obtaining gains through the antenna aperture. When analyzing the *impact* of MPCs on beamforming performance, the interplay between the antennas and propagation channel needs to be carefully considered, since it determines the achievable spectral efficiency through different beamforming techniques. However, these approaches require a dedicated up/down-conversion RF chain for each antenna element (to maximize the multiplexing gain), drastically increasing cost and energy consumption. To overcome this, *hybrid beamforming* has been proposed, which uses a combination of analog beamformers with digital beamforming via a *smaller* number of up/down-conversion chains. Numerous algorithms are devised in the literature for single- and multiuser systems (see [13] for a taxonomy). We note that multipath sparsity inherently complements the structure of the hybrid transceivers. However, with an increasing number of MPCs, systems designed for sparse channels do not perform as well. Figure 2b shows the ergodic spectral efficiency of a single-user multiple-input multiple-output (MIMO) system with the hybrid beamforming algorithm detailed in [14]. With 4 and 8 RF chains at each link end, the ergodic spectral efficiency of the system *saturates logarithmically* with an increasing number of clusters.

Spatial Consistency

Existing 3GPP channel models are based on the concept of a *drop* — a channel segment which represents a period of *quasi–stationarity*; that is, the large-scale parameters for generating the channel impulse response (CIR) are *constant* during the simulation period. Between *multiple* drops, the large-scale parameters have no *continuity*, and independence is assumed. 5G systems require a propagation model where the parameters *continuously evolve*, e.g., for performance prediction of beam tracking approaches as the UE moves along a trajectory. While the COST 259/273/2100 models have long enabled spatial consistency (SC), particularly through the concept of visibility regions, 3GPP only recently [4, 11] defined two procedures for SC, namely Spatial Consistency Models I (SC-I) and II (SC-II). SC-I applies an iterative algorithm to update the channel parameters, and the moving distance of the UE is limited by the correlation distance, which is specified in [4]. As an example, we provide one realization of SC-I for an NLoS UMi scenario at 28 GHz. The initial spatially

At mmWaves, an important characteristic is the relatively small number of dominant MPCs, in comparison to microwave frequencies. While significant diffuse scattering is anticipated from theoretical considerations, recent measurement campaigns in both indoor and outdoor environments have demonstrated that a high percentage of the received energy can be explained by discrete MPCs.

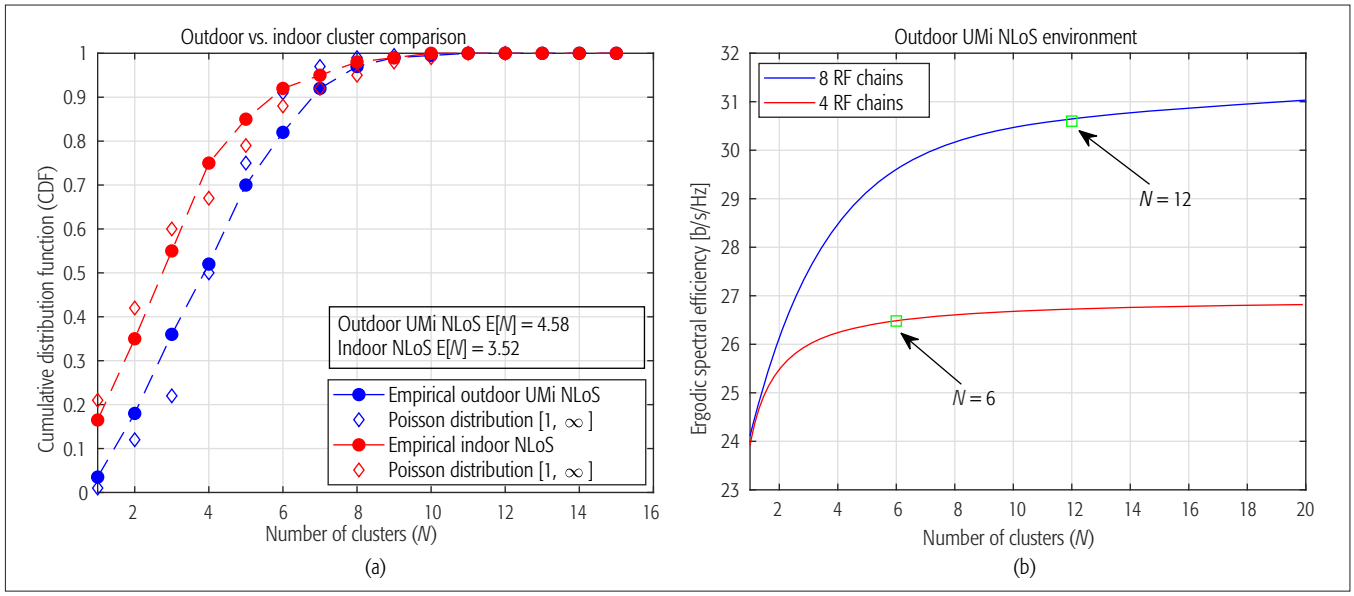

Figure 2. a) Measured and predicted number of clusters in an outdoor UMi NLoS and indoor NLoS environments at 28 GHz. The figure is reproduced from [12]; b) ergodic spectral efficiency of a single-user MIMO system vs. the number of clusters. The hybrid beamforming approach in [14] is employed.

consistent delays/powers/angles of clusters are generated according to the same procedure as without SC. Assuming the UE moves along a trajectory at a speed v, the moving distance will be limited within 1 m in a short time period Δt. Then, for each Δt interval, the delays, powers, and angles will be updated with the method in [4]. Finally, these updated parameters will be used to generate the CIR. The trajectory of the UE is plotted in Fig. 3a. There are *three* turning points, with the BS located at the starting *x-y* position. In Fig. 3b, the spatially consistent AoD variations can be seen with UE mobility.

Antenna Characteristics, Key Spatial Processing Differences, and Beam Management

Since the target is to support UE mobility, the antennas need to be *adaptive* in order to steer the gain toward the strongest scatterers or clusters of scatterers (i.e. to perform *analog beamsteering* with digital processing) in a coordinated fashion between BS and UE. This situation is different for most, but not all microwave systems, since they rely on time-division duplex (TDD) massive MIMO with full digital processing. Here, uplink pilots are used for downlink precoding, any antenna array geometry can be used, and the BS does not need knowledge of the incoming or outgoing channel directions.

At mmWave bands, the current assumption for 5G NR is that the BS regularly sweeps through *all* possible beam alternatives during a 5 ms interval, and the UE responds with a message directly after detecting its preferred beam alternative. There are *four* different beam management operations defined by the 3GPP:

- **Beam sweeping:** A sector is covered by a pre-defined set of transmitted and received beams in a time interval.
- **Beam measurement:** The BS or UE measure the quality of received beam (e.g., via SNR).
- **Beam determination:** The BS or UE selects its own beams.
- **Beam reporting:** The UE reports its measurement of beam quality to the BS.

In the 3GPP/ITU standardization, there are two basic array configurations defined for the BS for system-level performance evaluation: 8 × 8 and 16 × 16 planar arrays. Typically, dual polarization also needs to be considered. In the above cases, it is important to note that the resulting *array gain* depends on the *steering angle*. The half power beamwidth of a 256-element cross-polarized BS array with 45° slant angle configured in a 16 × 16 planar fashion is approximately 8° in both azimuth and zenith domains with a broadside directivity of 30.1 dBi. For UEs, it is also necessary to have adaptive arrays to close the link budget. It is important that the BS works in synchronization with the UE, such that their boresights are *aligned* as they jointly transmit/receive energy from scatterers. Critically at mmWaves, this needs to happen *independent* of the UE orientation. This implies that the UE has to constantly *track* the directions from which the power is coming in order to steer its beams and compensate for any movements by the user. In [15], a typical array response of a UE with and without influence of a person holding the device is shown, highlighting the beam distortion of close objects to the array. It is important to remember that the beamforming at the BS will affect the way the UE experiences the channel. Typically, the number of *effective* scatterers, the number of *visible* clusters, DS, and AS are reduced significantly as the BS only illuminates a part of the available channel during communication. This also means that alternative paths for the UE to lock on to during communication are reduced while the link is in operation.

Practical Challenges and Latest Industrial Developments

Practical Challenges

While a complete discussion of the relevant deployment challenges warrants a dedicated article, below we present some of the most important

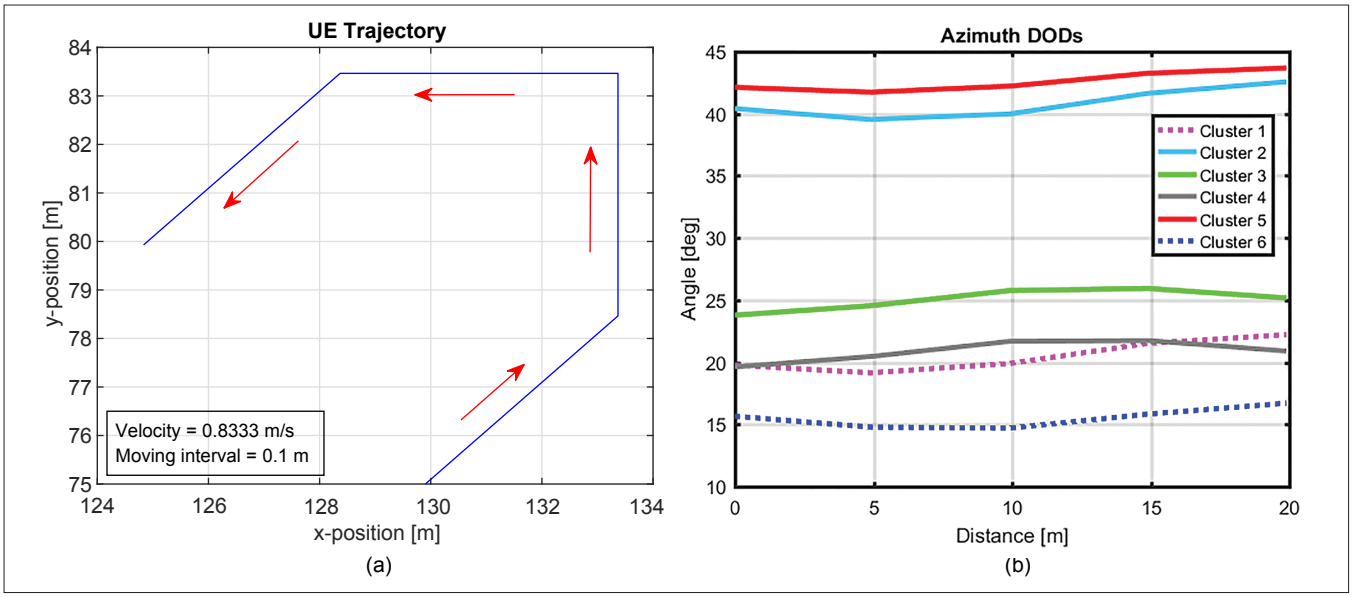

Figure 3. Illustrations of SC in an NLOS UMi scenario at 28 GHz. One realization of the SC–I process is considered from ITU — Radiocommunication Standardization Sector (ITU-R) M.2412: a) the BS is located at the starting x-y position at the beginning of the UE's moving trajectory; b) the azimuth AoD continuity vs. distance.

implementation difficulties of mmWave systems, and discuss their corresponding countermeasures.

- Deeper shadowing dips and larger outage regions are overcome by *network densification* accounting for the anisotropy of propagation in many relevant scenarios, and/or system layout that can fill mmWave coverage holes with underlying centimeter-wave (cmWave) connections, say LTE instead of non-standalone (NSA) 5G–NR.
- Large outdoor-to-indoor penetration loss for certain building materials (steel, concrete, energy-saving windows) can be solved by either *outdoor* placement for the mmWave antennas combined with cmWave distribution into the building, or *special coupling structures*.
- Increased sensitivity of beamforming to even *small* movement, both for beamforming based on instantaneous channel state information (CSI) (position changes in units of wavelength determine behavior), and average CSI (faster change of angular power spectra due to sharper shadows in mmWave systems), are combated by new algorithms for robust beamforming as well as extrapolation of channel characteristics, possibly with the help of location and channel information in the cmWave bands.
- Higher Doppler frequency and phase noise leads to larger inter-carrier interference in multi-carrier systems, and can be combatted by *optimized* multicarrier spacing or novel *modulation* methods such as orthogonal time frequency space (OFTS) modulation.
- Requirements of faster feedback (due to higher Doppler) are solved by either introduction of larger *link margins* or redesign of *frame/feedback structure*.

Latest Industrial Developments

The first commercial deployment of 5G systems will be in accordance with 3GPP Release 15 (NR), which was frozen in March 2018. Preferred bands for the initial deployment are *C–band (3.3–4.2 GHz) and 26/28 GHz*. Specifications have been developed, but only trials have been done thus far. Commercial deployments are expected to take place after World Radiocommunication Conference 2019. There are two deployment architectures for 5G systems: NSA and standalone (SA). The preferred architecture for *initial* deployment is NSA. Here, a 5G cell in *any* band is secondary to LTE and derives its control channel from an LTE cell. In SA deployment, a master node could be in the C–band and a secondary node in the mmWave band. The 3GPP Release 15 *SA* architecture was frozen in June 2018; however, more enhancements to some interfaces still need to be done. From the physical layer radio perspective, the C–band is expected to support TDD–based digital beamforming for simultaneous service to many UEs, while the 26/28 GHz bands are expected to support analog or hybrid beamforming to a relatively smaller number of UEs. While research has been done on exploiting the physical layer correlation of the propagation characteristics in the two bands, *we are not aware of systems that will be deployed in the near future with such tightly coupled radios.*

Conclusions

This article has summarized key differences between propagation at microwave vs. mmWave frequencies. Table 1 captures these differences and highlights their impact on 5G mmWave systems.

References

[1] T. S. Rappaport *et al.*, "Wideband Millimeter-Wave Propagation Measurements and Channel Models for Future Wireless Communication System Design," *IEEE Trans. Commun.*, vol. 63, no. 9, Sept. 2015, pp. 3029–56.
[2] K. Haneda *et al.*, "A Statistical Spatio-Temporal Radio Channel Model for Large Indoor Environments at 60 and 70 GHz," *IEEE Trans. Antennas and Propag.*, vol. 63, no. 6, June 2015, pp. 2694–2704.
[3] WINNER IST-4-027756 D1.1.2, "Part I — Technical Report on WINNER II Channel Models," *Wireless World Initiative New Radio*, Jan. 2007; http://www.ist-winner.org.

Parameter	Impact of frequency	Impact of bandwidth	Impact on 5G mmWave cellular systems
Path loss	Dependent on antenna gain Quadratic *increase* with decreasing area Quadratic *decrease* with constant area	N/A	May result in decrease/increase of cell range if antenna gains are not/are sufficient to compensate the propagation loss
Shadow fading	Increases with frequency; human induced shadow fading may also occur	N/A	Higher fade margins required for link budgeting
Delay spread	No clear trend More measurements needed	No clear trend More measurements needed	Direct impact unclear
Doppler Spread	Linear increase with frequency	No clear trend	Large inter-carrier interference in OFDM systems
Angular spread	No clear trend More measurements needed	No clear trend. More measurements needed	Small intra-cluster spreads reduces spatial degrees of freedom; SC yields inter-user correlation helping beam tracking but makes linear precoding less efficient
Multipath richness	Sparsity increases	More delays can be resolved	Hybrid beamforming approaches digital beamforming spectral efficiency with fewer RF chains for sparse channels
Ricean *K*–factor	No clear trend	No clear trend	Decreases the spatial degrees of freedom
LoS probability	N/A	N/A	Impacts the eigenvalue structure Also impacts the numbers of streams that can be efficiently multiplexed
Penetration loss	Increases with frequency	No clear trend	Decreases the cell range for outdoor-to-indoor links

Table 1. Summary of key differences between microwave and mmWave frequency bands, and their impact on 5G mmWave cellular systems.

[4] ITU-R M.2412-0, "Guidelines for Evaluation of Radio Interface Technologies for IMT-2020"; http://www.itu.int.
[5] S. Sun *et al.*, "Investigation of Prediction Accuracy, Sensitivity, and Parameter Stability of Large-Scale Propagation Path Loss Models for 5G Wireless Communications," *IEEE Trans. Vehic. Tech.*, vol. 65, no. 5, May 2016, pp. 2843–60.
[6] A. F. Molisch, *Wireless Communications*, 2nd ed., Wiley-IEEE Press, 2011.
[7] T. S. Rappaport *et al.*, *Millimeter Wave Wireless Communications*, Pearson/Prentice-Hall, 2015.
[8] A. Karttunen *et al.*, "Spatially Consistent Street-By-Street Path Loss Model for 28-GHz Channels in Micro Cell Urban Environments," *IEEE Trans. Wireless Commun.*, vol. 16, no. 11, Nov. 2017, pp. 7538–50.
[9] H. Okamoto, K. Kitao, and S. Ichitsubo, "Outdoor-to-Indoor Propagation Loss Prediction in 800-MHz to 8-GHz Band for an Urban Area," *IEEE Trans. Vehic. Tech.*, vol. 58, no. 3, Mar. 2009, pp. 1059–67.
[10] 3GPP TR 36.873 v.14.0.0, "Study on Channel Model for Frequency Spectrum Above 6 GHz," Jan. 2015; http://www.3gpp.org.
[11] 3GPP TR 38.901 v.14.3.0, "Study on Channel Models for Frequencies from 0.5 GHz to 100 GHz," Jan. 2018; http://www.3gpp.org.
[12] J. Ko *et al.*, "Millimeter-Wave Channel Measurements and Analysis for Statistical Spatial Channel Model in In-Building and Urban Environments at 28 GHz," *IEEE Trans. Wireless Commun.*, vol. 16, no. 9, Sept. 2017, pp. 5853–68.
[13] A. F. Molisch *et al.*, "Hybrid Beamforming for Massive MIMO: A Survey," *IEEE Commun. Mag.*, vol. 55, no. 9, Sept. 2017, pp. 134–41.
[14] O. El Ayach *et al.*, "Spatially Sparse Precoding in Millimeter-Wave MIMO Systems," *IEEE Trans. Wireless Commun.*, vol. 13, no. 3, Mar. 2014, pp. 1499–513.
[15] Y. Huo *et al.*, "5G Cellular User Equipment: From Theory to Practical Hardware Design," *IEEE Access*, vol. 5, July 2017, pp. 13,992–14,010.

Biographies

Mansoor Shafi (mansoor.shafi@spark.co.nz) received his B.S. and Ph.D. degrees from the University of Engineering and Technology at Lahore and the University of Auckland in 1970 and 1979, respectively. He is currently employed with Spark NZ and is an adjunct professor at Victoria University of Wellington. His research interests are in radio propagation models, transmission techniques, and novel cellular architectures.

Jianhua Zhang (jhzhang@bupt.edu.cn) received her B.S. from North China University of Technology in 1994 and her Ph.D. from Beijing University of Posts and Telecommunications in 2003, where she is currently a professor. Her research interests are massive MIMO and millimeter-wave channel modeling.

Harsh Tataria (h.tataria@qub.ac.uk) received his B.E. and Ph.D. degrees from Victoria University of Wellington in 2013 and 2017, respectively. He acquired a research fellowship at Queen's University Belfast and a visiting faculty member appointment at the University of Southern California in 2017 and 2018, respectively. His research interests include microwave and millimeter–wave transceiver design and radio propagation measurements.

Andreas F. Molisch (molisch@usc.edu) is the Solomon Golomb — Andrew and Erna Viterbi Chair Professor at the University of Southern California. He was previously at TU Vienna, AT&T (Bell) Labs, Lund University, and Mitsubishi Electric Research Labs. His research interests are in wireless communications, with emphasis on propagation channels, multi–antenna systems, ultrawideband systems, and localization.

Shu Sun (shu.sun@intel.com) received her B.S. degree from Shanghai Jiao Tong University in 2012 and her Ph.D. degree from New York University in 2018. She received the 2017 Paul Baran Young Scholar Award from the Marconi Society and the 2018 Dante Youla Award for graduate research excellence in electrical and computer engineering from NYU. She is now a systems engineer at Intel Corporation.

Theodore S. Rappaport (tsr@nyu.edu) received his Ph.D. degree from Purdue University in 1987. He is the David Lee/Ernst Weber Professor of Electrical and Computer Engineering with the New York University Tandon School of Engineering and the founding director of the NYU WIRELESS research center. He founded three major academic wireless research centers, has over 100 patents, and has published several hundred journal and conference articles and books.

Fredrik Tufvesson (fredrik.tufvesson@eit.lth.se) received his Ph.D. in 2000 from Lund University, Sweden. After two years at a startup company, he joined the Department of Electrical and Information Technology at Lund University, where he is now a professor of radio systems. His main research interest is the interplay between the radio channel and the rest of the communication system with various applications in the 5G ecosystem.

Shangbin Wu (shangbin.wu@samsung.com) received his B.S. degree in communication engineering from South China Normal University in 2009 and his M.Sc. degree from the University of Southampton, United Kingdom, in 2010. He received his Ph.D. degree from Heriot–Watt University, United Kingdom, in 2015. He joined Samsung R&D, United Kingdom, in November 2015. His research interests are propagation measurements and models for 5G systems.

Koshiro Kitao (kitao@nttdocomo.com) received his B.S., M.S., and Ph. D. degrees in electrical engineering from Tottori University, Japan, in 1994, 1996, and 2009, respectively. He joined the Wireless Systems Laboratories, Nippon Telegraph and Telephone Corporation (NTT), Kanagawa, Japan, in 1996. He is now a research engineer at NTT DOCOMO, INC., specializing in wireless propagation measurements and models.